Cyclic creep behaviour and strain classification of a bainite 2.25Cr-1Mo steel at 455ºC

Hao Jiang[1], Oluwadamilola Ogunmola[1], Zizhen Zhao[1], and Xu Chen[1]

[1]Tianjin University

July 13, 2020

Abstract

Uniaxial static and cyclic creep tests are carried out on a bainite 2.25Cr-1Mo steel at 455℃. The dependence of cyclic response on varied unloading conditions is investigated, with unloading rates from 0.6 MPa/s to 39 MPa/s and the valley stress duration from 0 to 30 min. Fracture surfaces of each specimen are analysed by using a scanning electron microscopy, and a systematic classification of strain components under cyclic creep is proposed to determine the actual damage. The results indicate that, the fracture modes under static and cyclic creep conditions both have ductile features. Due to the effect of anelastic strain recovery, the strain accumulation rate under cyclic creep is significantly retarded as compared with static creep, and the unloading conditions apparently influence the behaviour of anelastic strain recovery. Moreover, a life prediction method for cyclic creep tests based on mean actual strain deducted recovery strain is proposed.

Introduction

High temperature equipment is generally subjected to cyclic loadings during operation.[1-5] Hence, the failure mechanism of these kinds of equipment is complicated and often with mixed damages modes of creep, fatigue, as well as their interactions. Under realistic loading conditions, such as nuclear reactor components, stress loading is considered to be more common than strain loading.[6]Cyclic creep commonly refers to the progressive change of mean strain during the cyclic plastic deformation of a material between fixed stress limits, which belongs to creep-fatigue interactive behaviour.[7] Therefore, cyclic creep response of materials should be an essential consideration for the component's design.

The cumulative deformation for cyclic creep is time-dependent, which is similar to ratcheting.[8,9] According to previous studies, the strain rate can be greatly influenced by a series of test parameters, such as stress amplitude, stress ratio, and duration under hold stress. With the increase of duration under peak stress, a transition in dominant damage type from fatigue to creep can be found, and the fracture mode transformed from brittle to ductile failure correspondingly.[10] Moreover, research results of 9-12% Cr steel showed that the strain rate in cyclic creep was between those under ratcheting fatigue and static creep, i.e., the creep damage was more significant than fatigue damage, and the pure creep rate determined the upper rate of the cyclic creep.[11]Similar performances can be found in some nickel-based alloy such as GH720Li alloy[12] and MA754 alloy.[13]However, research on the cyclic creep response of a nickel-based super alloy DZ125 under different gradients of stress amplitudes and temperatures showed that cyclic creep led to accelerate the strain accumulation compared with static creep, and the ratcheting fatigue rate was reported to be the upper rate of the cyclic creep, even if the duration under peak stress was as long as 240 minutes.[14] Cases where fatigue damage dominates could also be found on pure metal copper[15] and AMg6 alloy.[16]In addition, a material appears opposite results at different temperature, such as Cr-Mo-V steel was observed cyclic creep acceleration at room temperature and cyclic creep retardation at 550 respectively.[17] Therefore, cyclic creep performances deserve more attention, and the underlying deformation mechanism should be further studied.

1

For creep-dominated cases, the anelasticity produced during unloading of cyclic creep is the main reason to retard the creep rate. Researchers have found that the anelasticity occurs if a material undergoes a sudden change in loading and requires time to attain a new equilibrium configuration.[18] Zhang et al.[19] analysed the anelastic strain of 9-12% Cr steel during different valley stress holding stages alongside with changed stress amplitudes, stress ratios, and peak stress durations. The results indicated that magnitude of anelastic strain increased with the increasing stress amplitude, peak stress duration and decreasing stress ratio. On the other hand, the research by Gaudin et al.[20] on 316 austenitic stainless steel found the reversibility of plastic strain reversibility, which inhibited cyclic creep below a threshold stress. Rao et al.[21] justified the relationship between the dislocation distribution and the anelastic behaviour by using a back stress division approach, together with observations from transmission electron microscopy (TEM). In addition, some microscopic mechanisms on the anelastic behaviour of pure metal and alloy also have been proposed, such as the bowing of dislocations between precipitates,[22] the grain boundary reverse slip due to the relaxation of dislocation pile-ups,[23] the reverse movement of dislocations in sub-grain,[24] and the reverse bending of sub-grain boundaries.[25,26] More recently, Hosseini et al.[27] proposed a simplified model of 9-12%Cr steel for the movement of dislocation pile-ups based on the effective stress concept.

Due to its good mechanical properties at elevated temperatures, 2.25Cr-1Mo steel has been extensively used in pressure vessels and pipeline systems in petroleum and power industries. The mechanical behaviour of 2.25Cr-1Mo steel under static creep, low cycle fatigue, and creep-fatigue interaction conditions have been studied by Klueh,[28] Jaske,[29] and Challenger et al.[30,31] Kschinka and Stubbins[32] conducted uniaxial fatigue and creep-fatigue tests at 565°C in both air and vacuum environments to understand the effects of waveform and environment on the fatigue behaviour of a forged bainitic 2.25Cr-lMo steel. Although large amounts of data have been available on creep-fatigue interaction of 2.25Cr-lMo steel, most of them are based on strain-controlled tests. Research on cyclic creep under stress-controlled and anelastic behaviour of 2.25Cr-1Mo steel has rarely been reported, and corresponding failure mechanism is still inexplicit as yet.

In this study, a series of uniaxial stress-controlled cyclic creep tests on bainite 2.25Cr-1Mo steel at 455°C in air are conducted, and the strain accumulation processes under different unloading conditions are analysed through the stress-strain curves. Specific attention is paid to the effect of unloading rate and duration under valley stress on the anelastic behaviour. Moreover, scanning electron microscopy (SEM) observations of fracture surfaces are performed to identify the failure mechanism. A life prediction method for cyclic creep under different unloading conditions is proposed based on the ductile exhaustion theory.

Experimental procedure

Material

The material used for this study is a bainite 2.25Cr-1Mo steel, with cyclic properties being reported in an earlier work.[33] The steel was normalized at 950 °C for 6 hours, and followed by tempering at 690 °C for 6 hours. Then simulated post-weld heat treatment was done at 690 °C for 8 hours, which was aimed to release residual stress. Fig. 1 (a) presents the microstructural morphology of the steel under an optical microscope (OP), and the metallographic structure is mainly granular bainite. The chemical composition of the steel is shown in Table 1. The material was machined into cylindrical test specimens for static creep and cyclic creep tests, with a diameter of and a gauge length of 50 mm, and the dimension specification is shown in Fig. 1 (b).

Table 1 The chemical composition of the bainite 2.25Cr-1Mo steel (wt %).

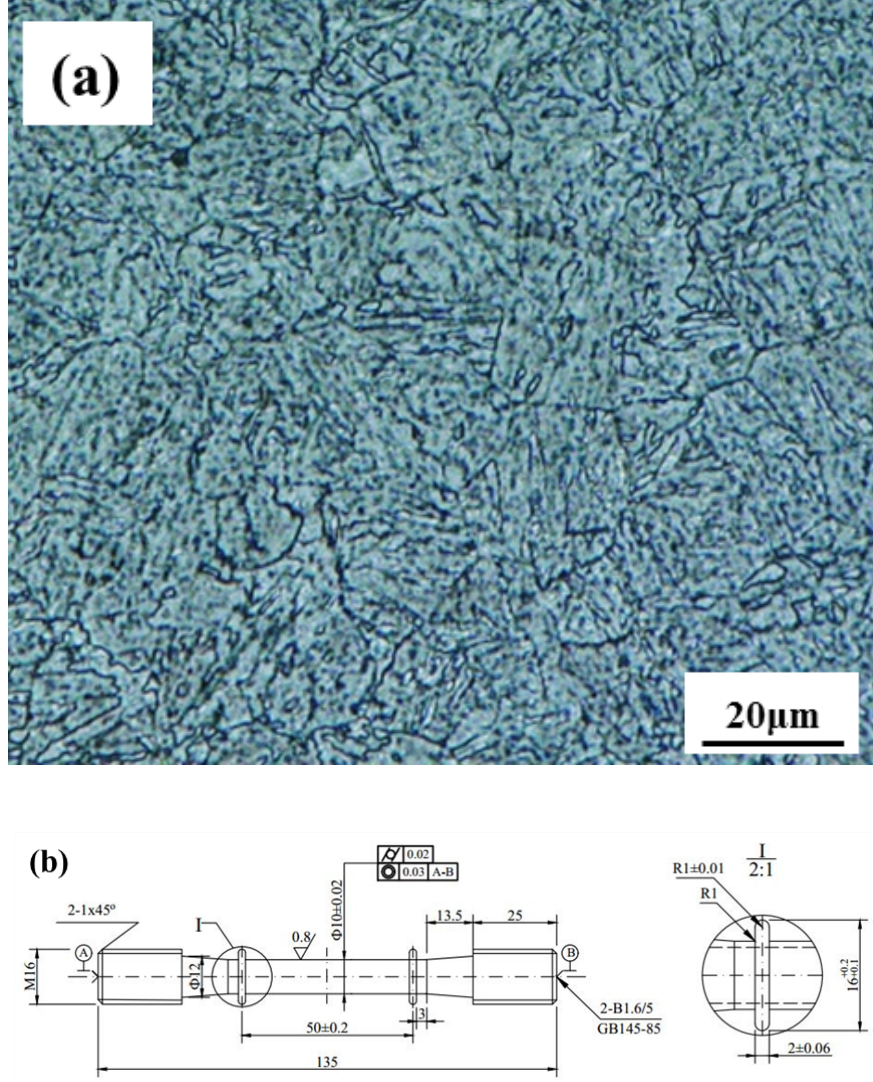| C	Si	Mn	P	S	Cr	Mo	Ni	Fe
0.15	0.05	0.48	0.006	0.002	2.42	0.96	0.08	Bal.

Fig. 1 (a) Metallographic structure of the bainite 2.25Cr-1Mo steel under OP and (b) the dimension specification of test specimen (in mm).

2.1 Cyclic test program

Uniaxial static creep and cyclic creep tests are carried out on an electronic creep testing machine RD-50, as shown in Fig. 2 (a). Three K-type thermocouples are uniformly distributed along the gauge section of the tested specimen, which is heated to 455 °C in air by a high-temperature heating furnace. A period of 30 minutes is held before loading to obtain the target temperature, within a fluctuation of ± 1 °C. The deformations recorded on the left and right sides of the gauge section (denoted by d_l and d_r) are measured by two sides of heat resistant rail-type extensometers correspondingly, with an accuracy of 1 μm. Hence, the actual deformation d can be determined by the mean value of d_l and d_r to reduce the error, and the engineering strain ϵ is obtained by the ratio of the actual deformation d and the initial gauge length L as:

$d = \frac{d_l + d_r}{2}$

$\varepsilon = \frac{d}{L} \times 100\%$

3

For cyclic creep tests, a uniaxial pulsating tension-tension wave is applied under stress control, as shown in Fig. 2 (b). The t_p and t_v are the durations imposed at peak and valley stresses respectively, with $\dot{\sigma}$ and $\dot{\sigma}'$ being the stress rates under loading and unloading. The peak stress $\sigma_{\max}$ is 400 MPa and the stress ratio R is 0.375. The loading condition is fixed at a loading rate of 12 MPa/s with a duration t_p of 60 min, but various unloading conditions are applied, with $\dot{\sigma}'$ being 0.6 MPa/s, 12 MPa/s, 19 MPa/s, 39 MPa/s and t_v being 0 min, 10 min and 30 min. The static creep test under 400 MPa is also performed as a comparison. All specimens are tested till fracture, and test results are summarized in Table 2. The endurance life is defined as total fracture time deducting loading, unloading and valley stress duration time.
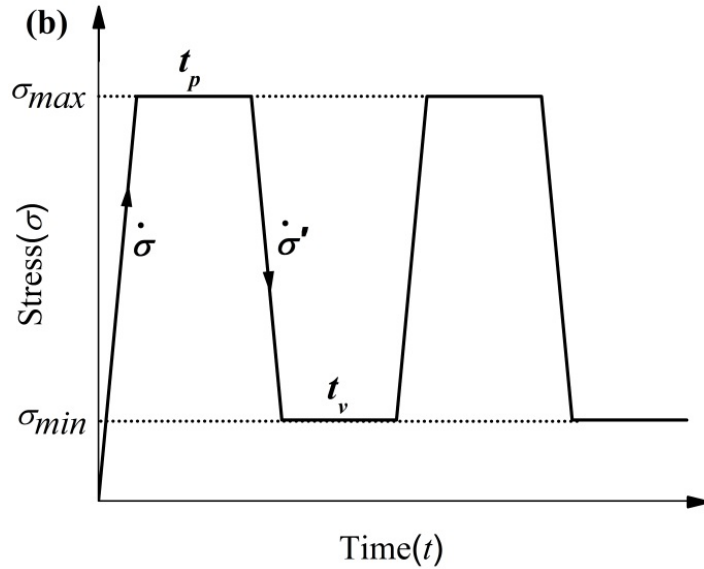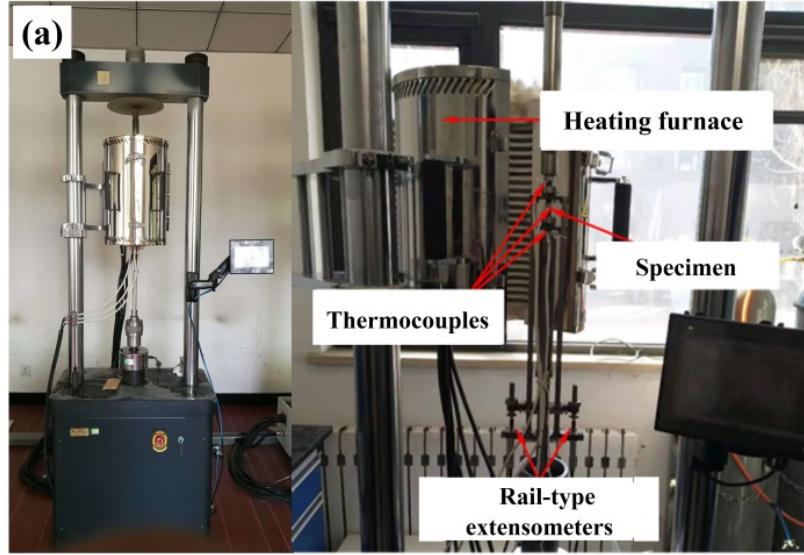

4

Fig. 2 Test conditions: (a) module of RD-50 electronic creep testing machine and (b) pulsating wave under stress-controlled.

Table 2 Summary of static creep and cyclic creep test results at 455.

Test type	Loading rate $\dot{\sigma}$ (MPa/s)	Duration of peak stress t_p (min)	Unloading rate $\dot{\sigma}'$ (MPa/s)	Unloading rate $\dot{\sigma}$
Static creep	12	infinite	-	-
Cyclic creep	12	60	0.6	0
			12	0
			19	0
			39	0
			12	10
			12	30

Results

3.1 Cyclic creep behaviour

Fig. 3 shows the variation of accumulated engineering strain with time under static creep and cyclic creep tests. The evolution of accumulated strain under all cyclic creep loadings in Fig. 3 (a) exhibit the similar three typical stages as static creep, which includes primary creep, secondary creep and tertiary creep stages. The primary creep stage of 2.25Cr-1Mo steel is quite short, and this feature has also been observed under the ratcheting-fatigue tests of 2.25Cr-1MoV steel.[34] However, the strain accumulation rate quickly decreases afterwards and keeps constant after entering the secondary creep stage, of which the constancy result from the equilibrium condition between strain hardening and recovery softening. The secondary creep stage accounts for nearly 80% of the endurance life and is also referred to as the stable stage. The comparison of static creep and cyclic creep within the initial 10 hours enclosed in a box in Fig. 3 (a) is presented in Fig. 3 (b). It also appears that the stable strain accumulation rate under cyclic creep is much lower than that under static creep, and this difference eventually leads to the significant increase of endurance life under cyclic creep. The retardation in the accumulation of strain under cyclic creep has also been found in other Cr-Mo steels[10, 35] and 316H austenitic stainless steel.[20] The width of strain range of cyclic creep is varied by unloading conditions, which leads to a difference in accumulation of strain since the first cycle and the difference is increased gradually. On the other hand, it has to be admitted that the increase in endurance life is partly occupied by loading, unloading, and valley stress dwelling under cyclic creep as compared with the static creep, which cannot be ignored especially in cases involving long durations of valley stress.

To unify the evaluation of life, the endurance life which refers to the total duration under the peak stress is proposed, and corresponding results are listed and compared in Table 2. Since the peak duration of a cycle is set as 60 min, i.e. one hour, the endurance life is approximately equal in value to the cycles to failure. The variations of endurance life with unloading rate and duration under valley stress are shown in Fig. 4 (a) and (b) respectively. The endurance life under static creep is still below that under cyclic creep, which confirms that 2.25Cr-1Mo steel under cyclic creep shows the prolongation effect on life compared with the static creep. Besides, the influence of prolongation effect changes with different unloading conditions. As shown in Fig. 4 (a), the endurance life grows with the increase of unloading rate when the duration of valley stress is none. The endurance life also increases with the extension of duration of valley stress when the loading and unloading rate is the same, as shown in Fig. 4 (b). The reasons for these two trends are discussed in detail later.
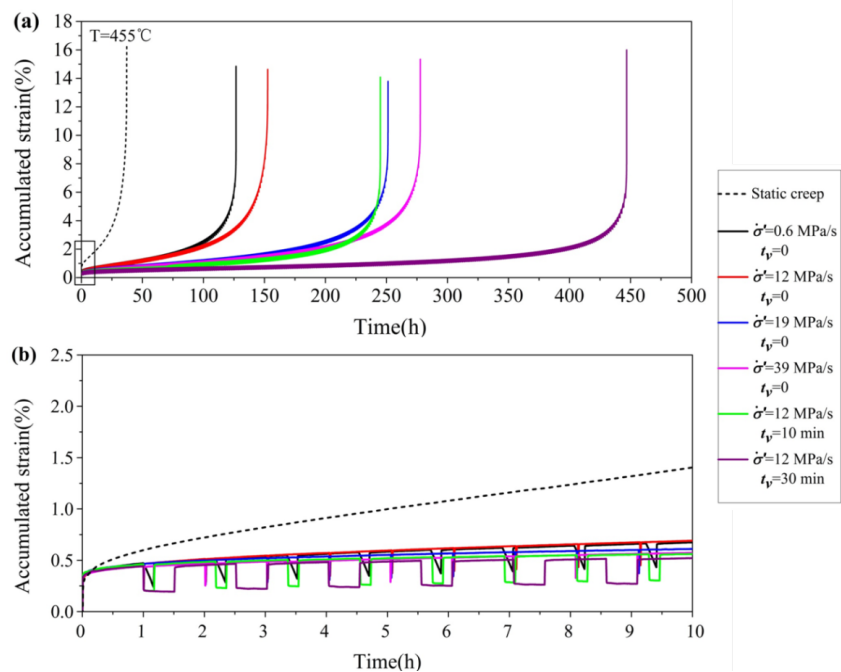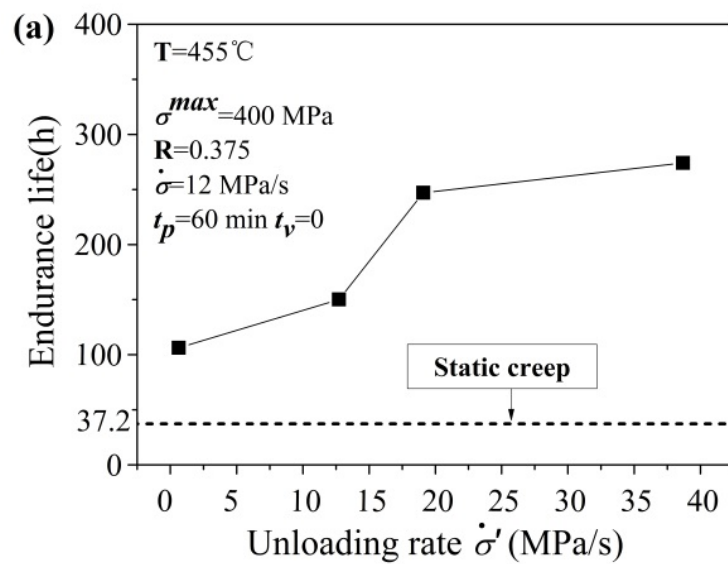
Fig. 3 (a) The strain-whole life curves under all test conditions and (b) comparison between static creep and cyclic creep within the initial 10 hours.
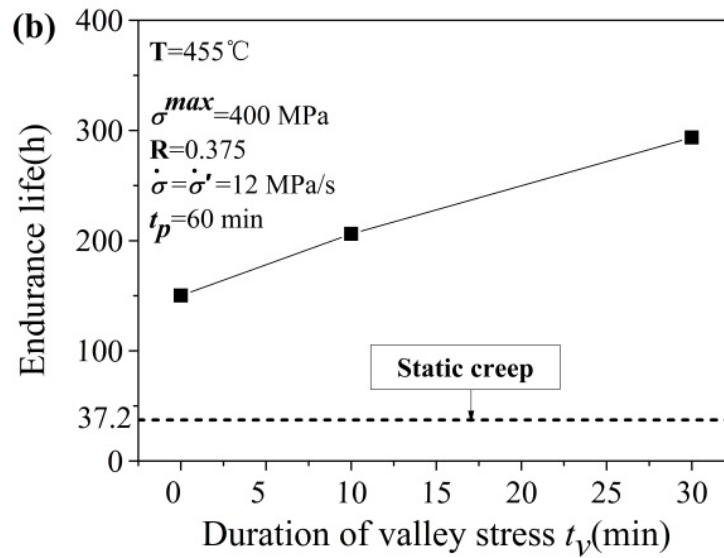
Fig. 4 The variation of endurance life with different (a) unloading rates and (b) durations under valley stress.

The elongation of all fractured specimens is analysed in Fig. 5. Cyclic creep loading leads to a slight drop in ductility as compared with static creep, but the difference in ductility under cyclic creep seems to have little influence on endurance life. Research results have shown that the fracture mode transforms from brittle type to ductile one and gradually approaches to static creep failure with the increase of duration under peak stress.[11] A quite long peak stress duration of 60 min has been imposed under all cyclic creep tests in present work, which means the fracture mode is most likely to be ductile, like static creep.
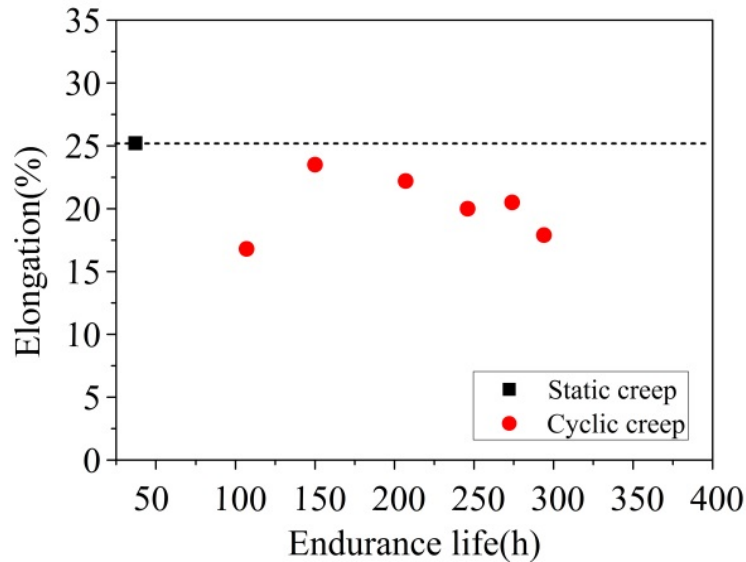

Fig. 5 Fracture elongation of specimen to the endurance life.

7

3.2 SEM observations

Typical SEM observations of the fractured surfaces after static creep and various cyclic creep tests are given in Fig. 6. All the fractured surfaces present a typical ductile failure feature, with a similar cup-cone shape of necking. Two different areas including (I) inner fibrous zone and (II) outer shearing lip can be found in Fig. 6 (a). Creep dimples and cavities located at the centre of the fibrous zone are shown in Fig. 6 (b). Second phase particles can be found in some cavities, as shown in Fig. 6 (c), and analysis results from energy dispersive spectrometer (EDS) indicate that these second phase particles tend to be $M_{23}C_6$ (Fe-Cr-C) carbides, which are precipitated from matrix α-Fe.[36,37] Comparing figures from Fig. 6 (d) to (g), the fibrous zone area under cyclic creep is found to suffer an obvious shrinkage compared with that under static creep, which may be resulted from the decrease of ductility. Besides, the distinct fatigue-creep cracks that are reported to be generated under cyclic loading in 9-12% Cr-Mo steels[38,39] are hardly detected in the examined 2.25Cr-1Mo steel, and the test environment in air and the relatively low frequency adopted in this work are likely to be the reason.
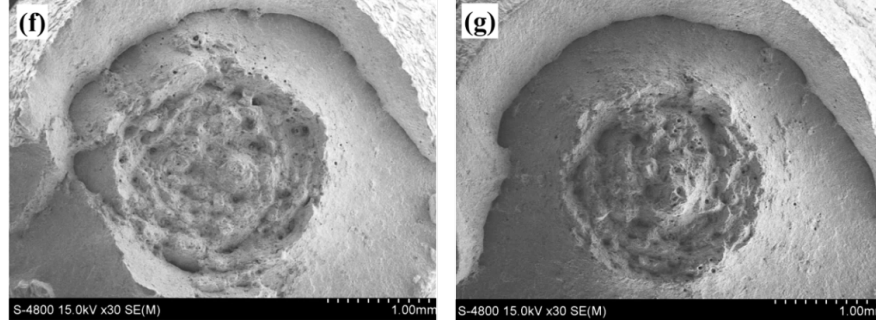

8
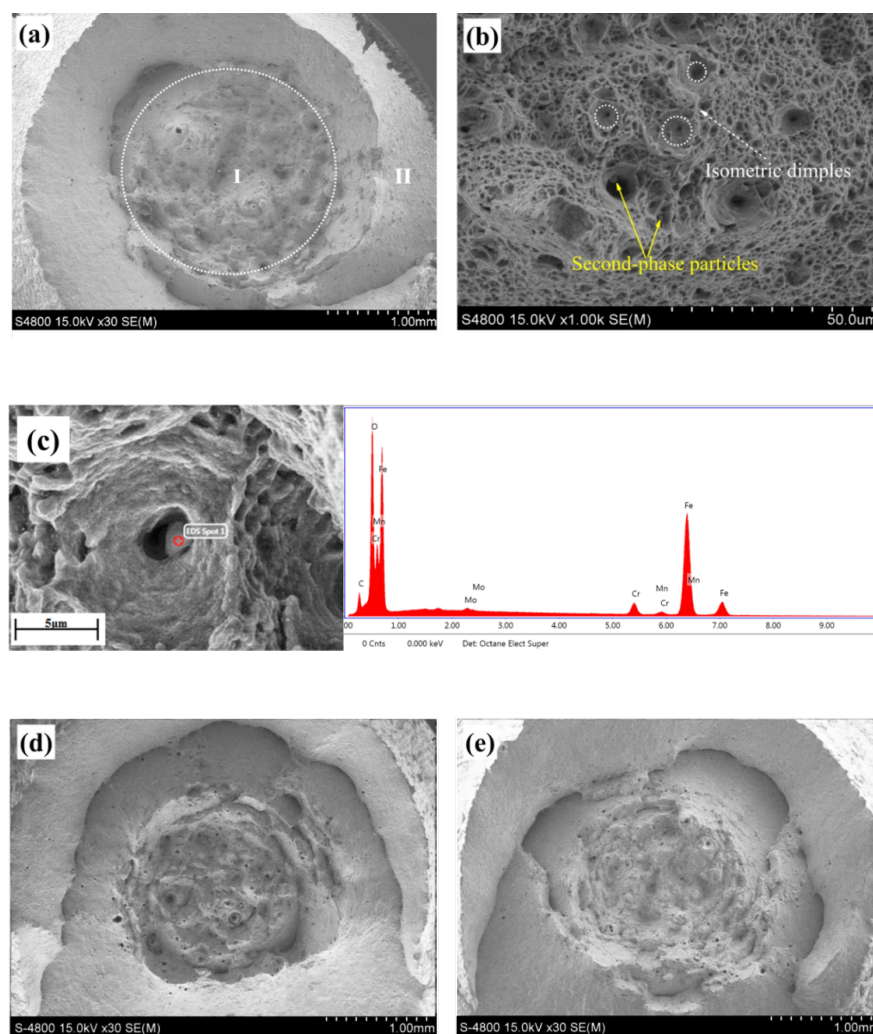
Fig. 6 SEM observations of fractured surfaces: (a) static creep and (b) enlarged inner fibrous zone; (c) second phase particle and (d) its composition; (e) cyclic creep at 12 MPa/s and 39 MPa/s unloading rate with none valley stress duration; (f) cyclic creep with 10 min and (g) 30 min duration under valley stress with an unloading rate of 12 MPa/s.

4. Discussion

4.1 Stress-strain curves

The typical stress-strain curve under cyclic creep is shown in Fig. 7, where $\sigma^{\max}$ and $\sigma^{\min}$ are of the peak and valley applied stresses, $\sigma_e^{\max}$ and $\sigma_e^{\min}$ are the upper and lower limits of the elastic domain respectively. The strain within the two adjacent cycles can be divided into four parts, as illustrated in Fig. 7 (a), including (I) ε^r, the ratcheting deformation which contains elastic and plastic strains, loading from the lower-elastic limit to the peak stress; (II) ε^c, which contains the creep strain generated during peak stress hold and a minor additional viscoplastic strain that is produced during the unloading process from peak stress to upper-elastic limit, In order to simplify the classification, the part of viscoplastic strain is considered as a continuation of creep. Previous works[40,41] have concluded that the viscoplasticity of materials has a contribution to creep during the loading and unloading stage; (III) ε^{re} , the total recovery strain when stress unloads from the upper-elastic limit to the valley stress and then reload to the lower-elastic limit; and (IV) ε^{act}, the actual increased deformation compared to the last adjacent cycle.
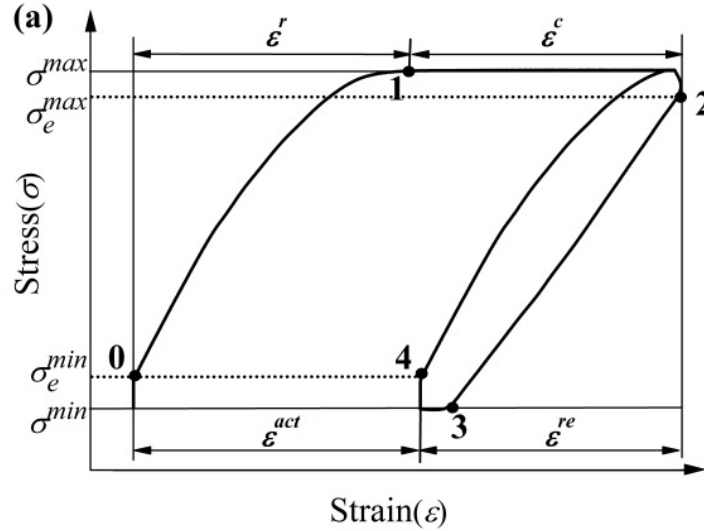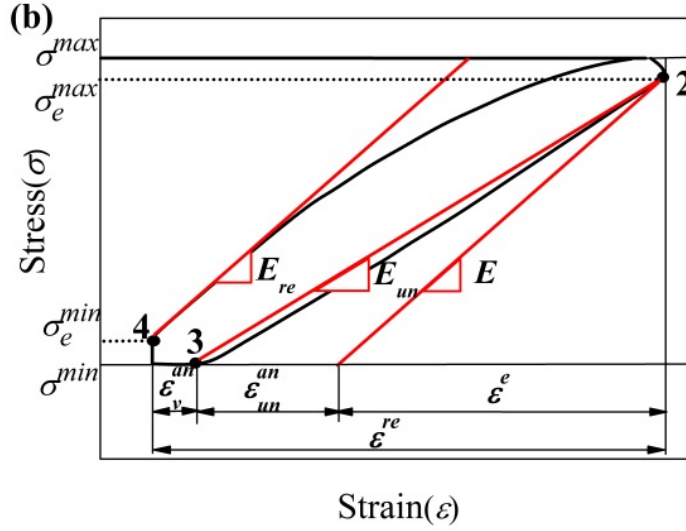
Fig. 7 Schematic diagram of classification of strains within two adjacent cycles.

As shown in Fig. 7 (b), the total recovery strain can be further divided into three parts by elastic modulus, i.e., (i) ε^e, (ii) $\varepsilon_{\mathrm{un}}^{\mathrm{an}}$, and (iii) $\varepsilon_v^{\mathrm{an}}$. The loading elastic modulus E and the reloading elastic modulus E_{re} correspond to the slope of the stress-strain curve in the elastic range. The unloading modulus E_{un}, considering its nonlinearity and complexity,[42,43] can be adequately defined by the straight line connecting the upper-elastic limit and the valley stress of the unloading stress-strain curve, which is similar to the fitting method of chord modulus in Kim et al.'s study.[44] Based on the difference between apparent modulus E_{un} and E , the component of anelastic strain $\varepsilon_{\mathrm{un}}^{\mathrm{an}}$ is separated during the unloading process. Considerably, the elastic recovery strain ε^e and anelastic strain $\varepsilon_{\mathrm{un}}^{\mathrm{an}}$ arise simultaneously rather than separately in reality.[45] Moreover, when stress is unloaded to the valley stress, it is observed that the strain can still spring back until the stress is reloaded to the lower-elastic limit. This part of the micro-plastic strain $\varepsilon_v^{\mathrm{an}}$ under the low-stress region is regarded as the major anelastic recovery in case with long duration under valley stress.[13] The two parts of anelastic recovery strain indicate the existence of a two-stage spring-back phenomenon when the applied stress is removed, which is closely related to the change of elastic modulus[46] and the movement of dislocations.[47]

The above values of strain can be obtained from experimental data, and the relationships are presented as the following:

$$
\begin{cases}
& \varepsilon_{\mathrm{un}}^{\mathrm{an}} = \varepsilon_2 - \varepsilon_3 - \varepsilon^e \\
& \varepsilon_v^{\mathrm{an}} = \varepsilon_3 - \varepsilon_4 \\
& \varepsilon^{\mathrm{re}} = \varepsilon^e + \varepsilon_{\mathrm{un}}^{\mathrm{an}} + \varepsilon_v^{\mathrm{an}} \\
& \varepsilon^{\mathrm{act}} = \varepsilon^r + \varepsilon^c - \varepsilon^{\mathrm{re}} = \varepsilon_4 - \varepsilon_0
\end{cases}
$$

where ε_0, $\varepsilon_1, \varepsilon_2$, ε_3 and ε_4 refer to the strains at different time points, and the values of $(\varepsilon_2 - \varepsilon_3)$ and ε^e can be calculated by the following equations:
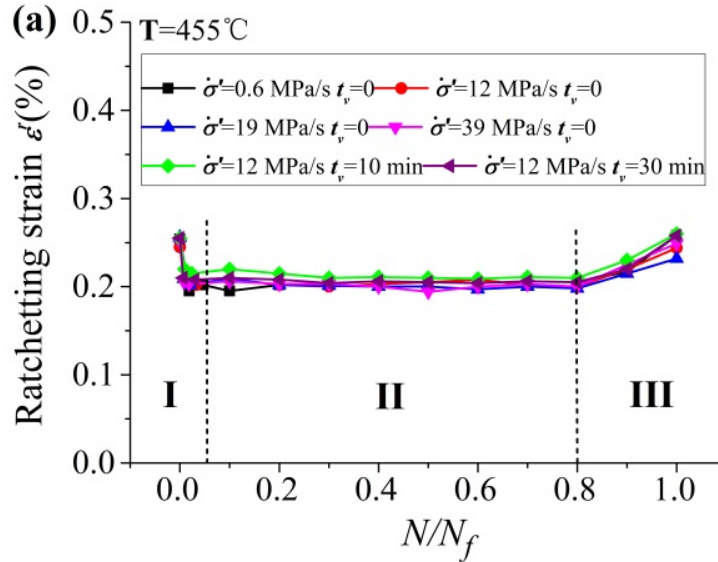
$$\varepsilon_2 - \varepsilon_3 = (\sigma_e^{\mathrm{max}} - \sigma^{\mathrm{min}})/E_{\mathrm{un}}$$

$$\varepsilon^e = (\sigma_e^{\mathrm{max}} - \sigma^{\mathrm{min}})/E$$

10

According to the above systematic classification, it can be found that the retardation effect in strain accumulation rate under cyclic creep results from the interaction between the strain (ε^r, ε^c) and recovery strain (ε^e, ε^{an}_{un}, and ε^{an}_v), or rather the anelastic recovery plays a vital role in recovering the previous inelastic deformation. Thereby, it is clear that the ultimate unrecovered strain is the actual damage created within two adjacent cycles, and the difference of retardation effect under varied unloading conditions can be studied by analyzing each part of the strain quantitatively.

Maximum strain in one cycle

4.2.1 Ratcheting strainε^r

The ratcheting strain ε^r is defined as the total elastic and plastic strain produced by loading from the lower-elastic limit to the peak stress. The evolution of ratcheting strain during the entire life (the values come from the first three cycles and $0.1N_f$, $0.2\ N_f$, $0.3\ N_f$, ..., $1N_f$, both here and below) under different unloading rates is shown in Fig. 8 (a). The developments of ratcheting strain follow the same trend under different unloading conditions. The evolution of ratcheting strain can be divided into three stages, where it is slightly large at first cycle, then drops to a stable value, and increases again before fracture. Moreover, the elastic component of the ratcheting strain can be obtained conveniently, which is inversely proportional to the loading elastic modulus E, as shown in Fig. 9 (a). The loading elastic modulus is hardly affected by changed unloading rate and the duration under valley stress. The evolution of loading elastic modulus also displays three stages, which shows that the value of E is large at the first cycle, then rapidly drops to a stable value, and further declines before fracture. It is found that both ratcheting strain and loading elastic modulus just enter the stable stage after the first cycle, which is related to the variation of dislocation. The degeneration of the loading elastic modulus is mainly due to the increase of dislocation density,[44,46] and the multiply of dislocations can cause a hardening effect for the plastic component of the ratcheting strain. It seems that the dislocation density has significantly increased within the first cycle by the initial loading and a long-term hold of peak stress, and the dislocation density may remain almost unchanged subsequently. Hence, the slightly large ratcheting strain at the first cycle can be attributed to the considerably large plastic component and small elastic component. In addition, the specimens exhibit remarkable necking near fracture, which leads to an increase of the ratcheting strain and a further decrease of the elastic modulus.
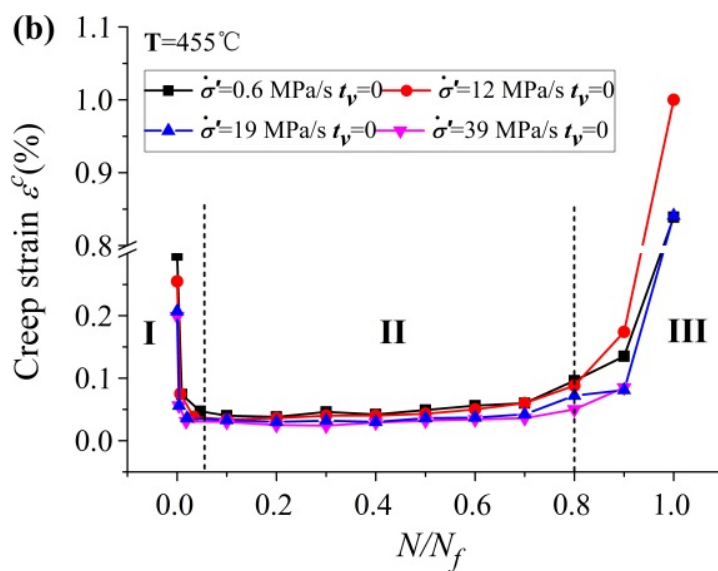
(b)

T=455°C

Creep strain ε^c (%)

Legend:
- $\dot{\sigma}'$=0.6 MPa/s t_v=0
- $\dot{\sigma}'$=12 MPa/s t_v=0
- $\dot{\sigma}'$=19 MPa/s t_v=0
- $\dot{\sigma}'$=39 MPa/s t_v=0

I   II   III

N/N_f

Fig. 8 Evolutions of the strain during the entire life under different unloading conditions: (a) ratcheting strain and (b) creep strain.

(a)

T=455°C

Loading elastic modulus E(GPa)

Legend:
- $\dot{\sigma}'$=0.6 MPa/s t_v=0
- $\dot{\sigma}'$=12 MPa/s t_v=0
- $\dot{\sigma}'$=19 MPa/s t_v=0
- $\dot{\sigma}'$=39 MPa/s t_v=0
- $\dot{\sigma}'$=12 MPa/s t_v=10 min
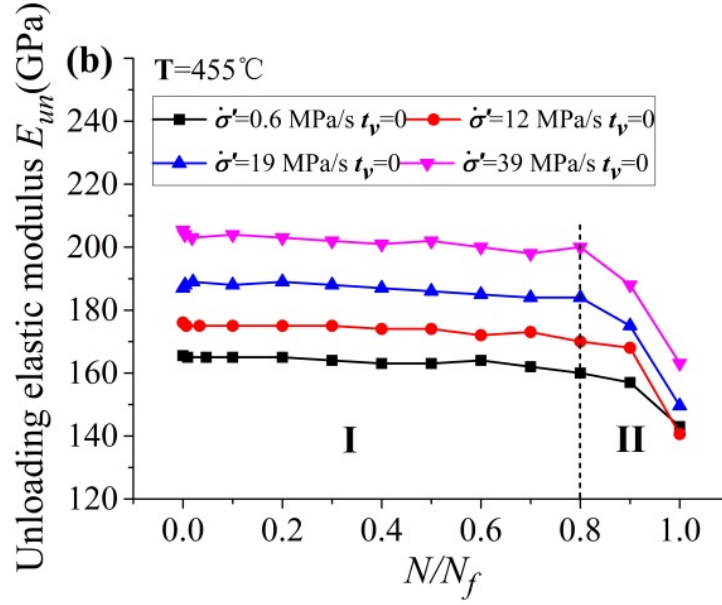- $\dot{\sigma}'$=12 MPa/s t_v=30 min

I   II   III

N/N_f

12
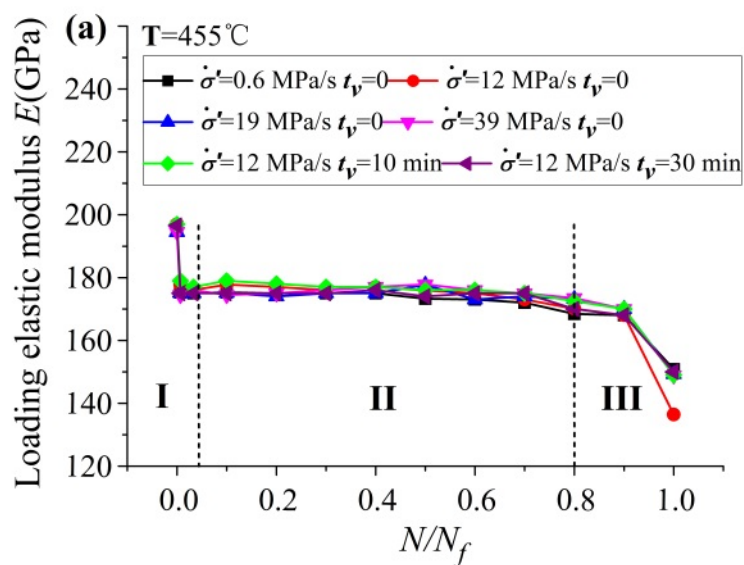
Fig. 9 Evolutions of elastic modulus during the entire life under different unloading conditions: (a) loading and (b) unloading.
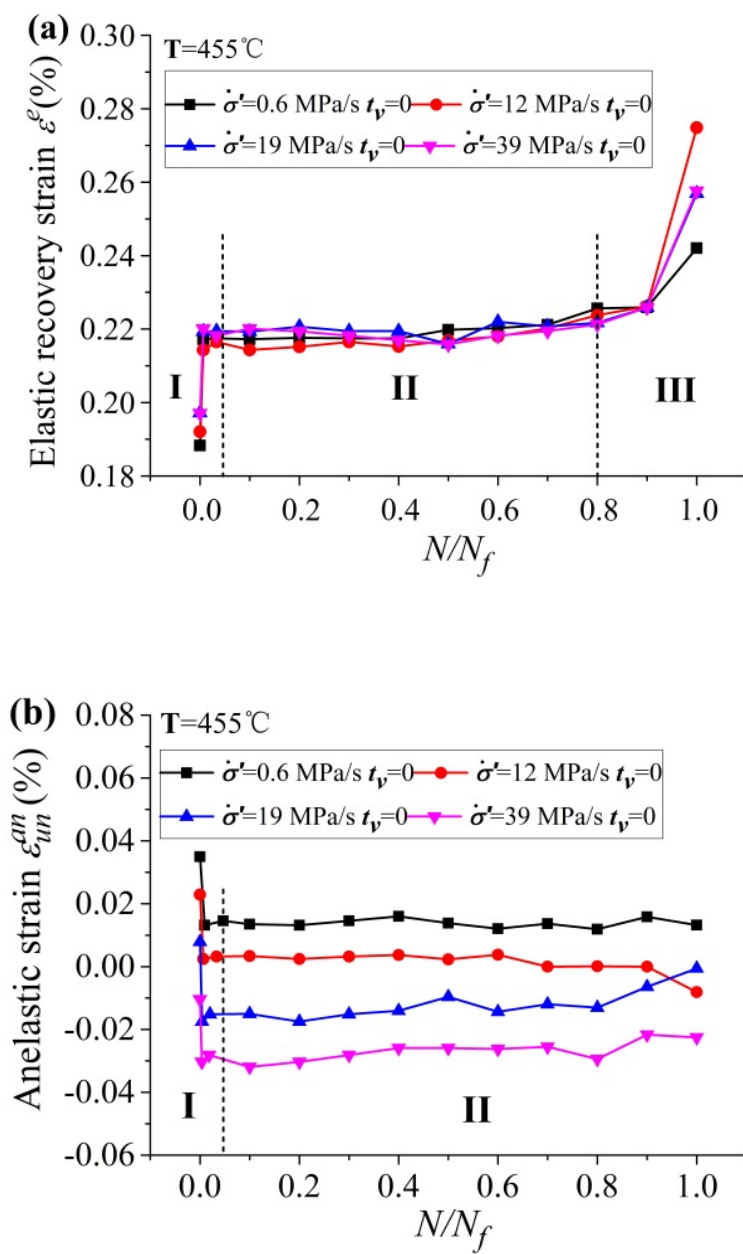
4.2.2 Creep strain ε^c

As above classification, the creep strain ε^c is calculated by the sum of the deformation during the peak stress hold time and a minor additional viscoplastic strain near the peak stress. As shown in Fig. 8 (b), the evolution of ε^c displays three stages obviously, as the creep strain decreases sharply after the first cycle and then keeps constant before increases again near fracture. The difference of the creep strain would result from the viscoplastic component, which can be affected by the changed unloading rate.

The maximum strain in one cycle is the sum of the ratcheting strain ε^r and creep strain ε^c as shown in Fig.7 (a).

Recovery strain ε^{re} in one cycle

4.3.1 Elastic recovery strain ε^e

Fig. 7 exhibits that the strain starts to reverse as the stress drops to the upper-elastic limit, which indicates the strain begins to recover. The elastic recovery strain ε^e mainly depends on the loading elastic modulus E and the upper-elastic limit $\sigma_e^{\max}$, which can be calculated according to Eq. (5). The values and evolution of the loading elastic modulus have been mentioned and displayed in Fig. 9 (a). The upper-elastic limit can be obtained by applied peak stress and viscous stress according to Eq. (6). Therefore, the elastic recovery strain for different unloading rates is obtained in Fig. 10 (a), which also shows three distinct stages. The elastic recovery strain is slightly large for high unloading rate at the first cycle and then keeps constant with little difference in the stable stage before increases again at last. It means that the value of ε^e depends on the loading elastic modulus mainly and is hardly affected by the difference of the upper-elastic limit within the examined range of unloading rates.
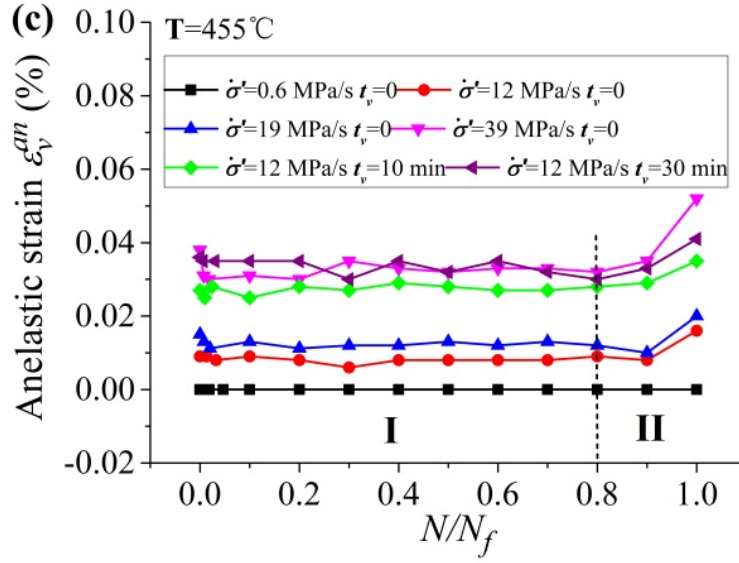
13

(a)

T=455℃

Legend:
- $\dot{\sigma}'$=0.6 MPa/s t_v=0 (black square)
- $\dot{\sigma}'$=12 MPa/s t_v=0 (red circle)
- $\dot{\sigma}'$=19 MPa/s t_v=0 (blue triangle)
- $\dot{\sigma}'$=39 MPa/s t_v=0 (magenta inverted triangle)

Y-axis: Elastic recovery strain ε^e(%)

X-axis: N/N_f

Regions: I, II, III

(b)

T=455℃

Legend:
- $\dot{\sigma}'$=0.6 MPa/s t_v=0 (black square)
- $\dot{\sigma}'$=12 MPa/s t_v=0 (red circle)
- $\dot{\sigma}'$=19 MPa/s t_v=0 (blue triangle)
- $\dot{\sigma}'$=39 MPa/s t_v=0 (magenta inverted triangle)

Y-axis: Anelastic strain ε_{un}^{an} (%)

X-axis: N/N_f

Regions: I, II

14

Fig. 10 Evolutions of the recovery strain ε^e during the entire life for different unloading rates: (a) elastic recovery strain (b) anelastic recovery strain of unloading stage and (c) anelastic recovery strain near valley stress.

4.3.2 Anelastic recovery strain of unloading stage ε_{un}^{an}

It should be noted that the anelasticity of Cr-Mo steels is complex.[18] To discuss the performance of anelastic recovery strain, it is generally agreed that the anelastic displacements are mainly related to the bowing of pinned dislocations, and the recoverability mechanism is due to the line tension. The line tension results in back stress that can bring dislocation lines back to their equilibrium position. Thus, based on the force equilibrium condition, the anelastic slip of a population of pinned dislocation lines during the recovery period can be described by simplified micromechanical modelling[48]:

$$\dot{\varepsilon^{an}} = \frac{b}{f}\left(m\frac{\varepsilon_0^{an}-\varepsilon^{an}}{l^2} - \rho_m\tau^{eff}\right)$$

where b is the Burgers vector, m is the material factor, f is the coefficient of internal friction, $\dot{\varepsilon}^{an}$ is the anelastic reverse slip rate, together with ε_0^{an} and ε^{an} refer to the slip displacement along applied stress direction and anelastic reverse slip displacement of dislocation respectively. l and ρ_m represent the length and the density of the dislocation respectively. It should be noted that ρ_m is assumed to be constant in this law, and τ^{eff} is the effective force to drive the deformation, which is related to the applied stress. Moreover, the former term of this equation is related to the back stress, which is found to be decreasing with the increase in the anelastic reverse slip displacement.

The anelastic recovery strain includes two parts as mentioned in the above classification. For the anelastic recovery strain of unloading stage ε_{un}^{an}, the unloading elastic modulus E_{un} under different unloading rates are obtained to make a comparison with the loading elastic modulus E. As shown in Fig. 9 (b), the evolution of E_{un} displays just two stages, which keeps stable initially with a slight decrease and finally declines a lot before fracture. The value of unloading elastic modulus is quite sensitive to the unloading rate, and it increases greatly with the increase in the unloading rate. Thus, the value of ε_{un}^{an} can be calculated by Eq. (3)-(5) and shown in Fig. 10 (b), where it decreases with the increase of unloading rate and maintains a constant value after the first cycle. It should be noted that when the unloading rate exceeds 20 MPa/s, ε_{un}^{an} will change to be negative. It is due to the method of classification and calculation, rather than the change of the dislocation slip direction. According to the Eq. (6), if the unloading rate increases during the unloading

15

stage, the effective stress will fall faster correspondingly, and the anelastic reverse slip displacement is less within a shorter time of unloading and causing more back stress being remained. Also, according to previous work,[49] the less internal friction measured by dynamic mechanical Analysis (DMA) was observed on 2.25Cr-1Mo steel in the case of higher frequency, hence the friction coefficient f would reduce with the increase of unloading rate and cause the high resulted anelastic slip rate corresponding to the valley stress.

4.3.3 Anelastic recovery strain near valley stress ε_v^{an}

The anelastic recovery strain near valley stressε_v^{an} represents the further reverse slip displacement of pinned dislocation after the unloading stage, which corresponds to the range between the valley stress and the lower-elastic limit. Fig. 11 shows the initial part of the reloading stress-strain curves of the 2nd cycle under different unloading conditions. The starting points of all curves are shifted and superimposed at the valley stress point.

In the case with none duration of valley stress, as shown in Fig. 11 (a), the anelastic recovery strain ε_v^{an}increases significantly with the increase of unloading rate, which is opposite to the trend of ε_{un}^{an}. It can also be explained by Eq. (6). According to discussions in 4.3.2, the larger the unloading rate, the more back stress is retained after unloading stage, when the anelastic reverse slip rate is high as well. Therefore, the dislocation can be derived backward for a more prolonged displacement. Moreover, the lower-elastic limit is the critical stress of the recovery behaviour, and it is also found to grow slightly with the increase in the unloading rate. For comparison in Fig. 11 (b), where the unloading rates are constant, the anelastic recovery strain develops with extended durations under valley stress. However, the increment extent of the anelastic strain decreases when the duration of valley stress is more than 10 min, which validates that the anelastic strain can be saturated with time as have been reported in other studies.[18,50] Fig. 10 (c) summarizes the anelastic recovery strain near the valley stress ε_v^{an}under different unloading conditions, which shows two stages, and the values all maintain constant during most of the life. Besides, it's interesting to find that the ε_v^{an} for quite a long duration of valley stress ($\dot{\sigma}'$=12 MPa/s,t_v =30 min) is closely equal to the instantaneousε_v^{an} under large unloading rate ($\dot{\sigma}'$=39 MPa/s, t_v =0 min). This indicates the performance of dislocation slip displacement, which mainly depends on the driving force and the slip time.
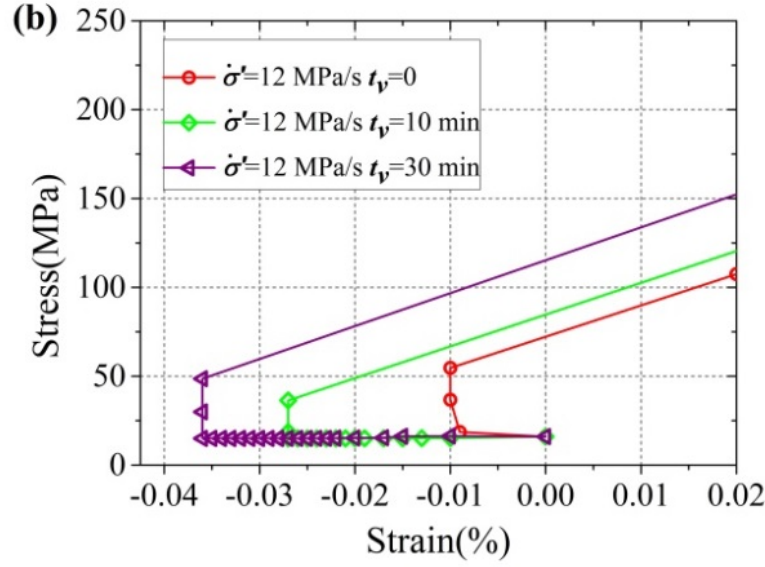

16
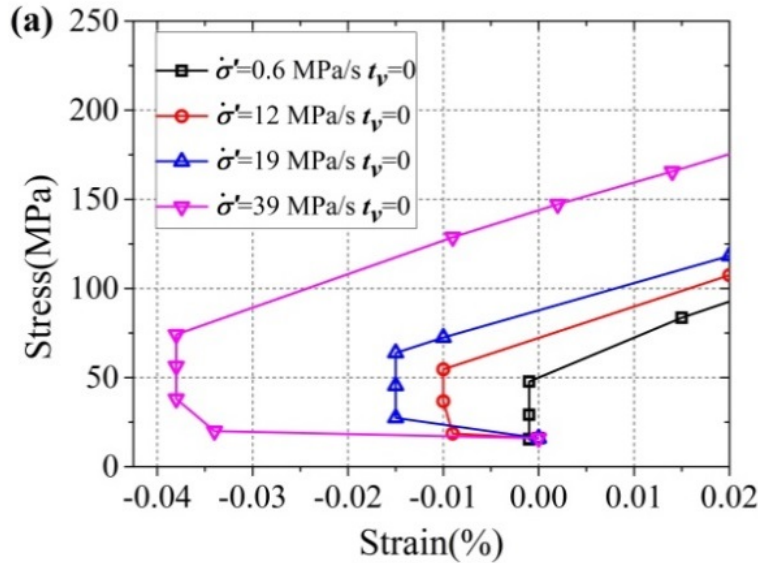
Fig. 11 Initial part of reloading stress-strain curves in the 2$^{\text{nd}}$ cycle under different unloading conditions: (a) unloading rates and (b) durations of valley stress.

The recovery strain ε^{re} is sum of the elastic recovery strain ε^{e}, anelastic recovery strain of unloading stage $\varepsilon_{\text{un}}^{\text{an}}$ and anelastic recovery strain near valley stress $\varepsilon_{v}^{\text{an}}$, as shown in Fig.7 (b).

5. Life prediction

In terms of the life prediction of creep-fatigue tests, the methods based on stress control are obviously fewer than strain control due to the unclosed hysteresis loops.[51,52] The ductility exhaustion approach in R5[53] is one of the wide-used life prediction methods of creep-fatigue tests under stress control, which describes the creep damage per cycle as:

$$d_c = \int_0^{\text{th}} \frac{\dot{\varepsilon}_{\text{in}}}{\varepsilon_f(\dot{\varepsilon}_{\text{in}}, \ T)} \mathrm{d}t$$

where $\dot{\varepsilon}_{\text{in}}$ is the inelastic strain rate of the material during the holding time per cycle, ε_f is the creep ductility of the material, which is usually related to the creep strain rate and temperature. Correspondingly, the fatigue damage per cycle is calculated by

$d_f = \frac{1}{N_f}$

where N_f is the fatigue life. When the sum of cumulative creep damage and fatigue damage is equal to 1, the failure is acknowledged and the predicted life of the creep-fatigue test is calculated as:

$N_p = \frac{1}{d_c + d_f}$

It should be noted that fatigue damage was confirmed to have little effect compared with creep damage under cyclic creep in present work. Hence, the term can be neglected, and the predicted result by the ductility exhaustion method of R5 is shown in Fig. 12. It can be found that the predictions are much lower than experimental results, and the error enlarges with the increasing observed cycles to failure. The predicted cycles to failure in the cases of long duration under valley stress are more outrageous, which are circled in red. The over-conservative prediction is generally due to the neglect of the anelastic recovery effect in cyclic creep.
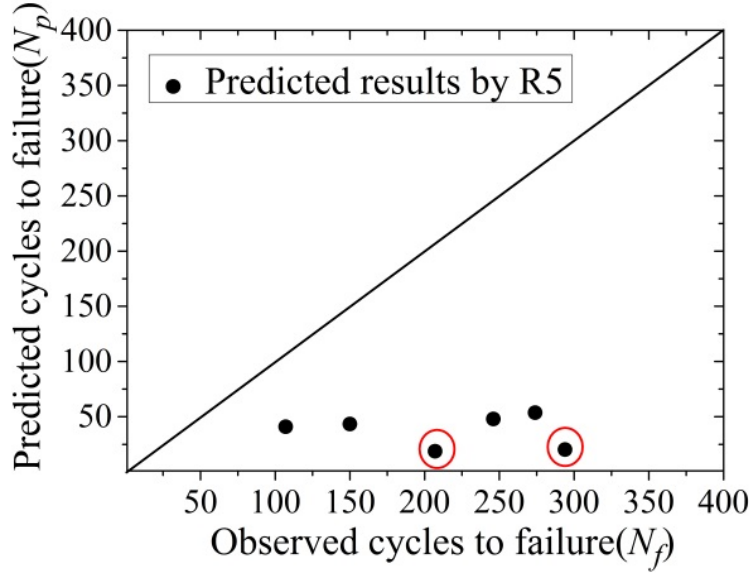
17

Fig. 12 Comparison of predicted and observed cycles to failure in cyclic creep by the ductility exhaustion method of R5.

According to the above study on each component of strain under cyclic creep, the mean values of the maximum strain and the recovery strains during the stable stage can be obtained, and their difference can be considered as the mean actual damage created per cycle$\varepsilon_m^{\mathrm{act}}$, as shown in Fig. 13.
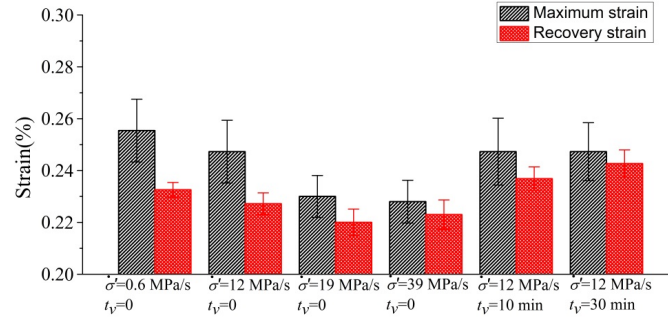

Fig. 13 Summary of mean values of the maximum strain and the recovery strain during stable stage under different unloading conditions.

Thus, based on ductile exhaustion theory, the damage per cycle of cyclic creep can be expressed as:

$$\frac{\mathrm{dD}}{\mathrm{dN}} = \frac{1}{\varepsilon^f}\frac{d\varepsilon^{\mathrm{act}}}{\mathrm{dN}} = \frac{1}{\varepsilon^f}\frac{d(\varepsilon^r + \varepsilon^c - \varepsilon^{\mathrm{re}})}{\mathrm{dN}}$$

where ε^f is the fracture strain of failed specimen, the sum of ε^r and ε^c is the maximum strain, and $\varepsilon^{\mathrm{re}}$ is the total recovery strain as mentioned above. It should be noted that the ductilityε^f is assumed to follow a power law relationship with the mean actual damage per cycle $\varepsilon_m^{\mathrm{act}}$ during the stable stage, thus a simple prediction equation can be obtained as:

$$N_f = \alpha(\varepsilon_m^{\mathrm{act}})^\beta$$

18

where α and β are fitting constants, which depends on material type. As shown in Fig. 14 (a), the relationship between N_f and $\varepsilon_m^{\mathrm{act}}$ under different unloading conditions can be well expressed by Eq. (11) in the double logarithmic coordinates, where $\alpha=14.431$, $\beta=-0.577$. Comparison of predictions and experimental results by modified approach is shown by black dots in Fig. 14 (b). It can be observed that all the accuracy of the estimation results is vividly improved, which fall within a scatter band of ±1.5.

It can be further speculated that, if a creep-fatigue test under stress control meets the condition that the stable stage occupies most of fatigue life, the actual damage of the stable stage obtained by strain classification method can still estimate the cycles to failure, regardless of the changed test conditions, such as peak stress, stress ratio, loading and unloading rate and the duration of peak or valley stress. The data of bainite 2.25Cr1MoV steel with short-term duration of hold stress and negative stress ratio at 455 °C is used to check the suitability of the proposed model[34]. The blue square points of Fig. 14 (b) presents the comparison of predicted and experimental results, where all the predicted results fall within a scatter band of ±1.5. Therefore, the mean actual damage can excellently reflect the essential strain accumulation process under various stress controlled test conditions, and it can be used as a single parameter of a prediction model with a satisfactory accuracy.
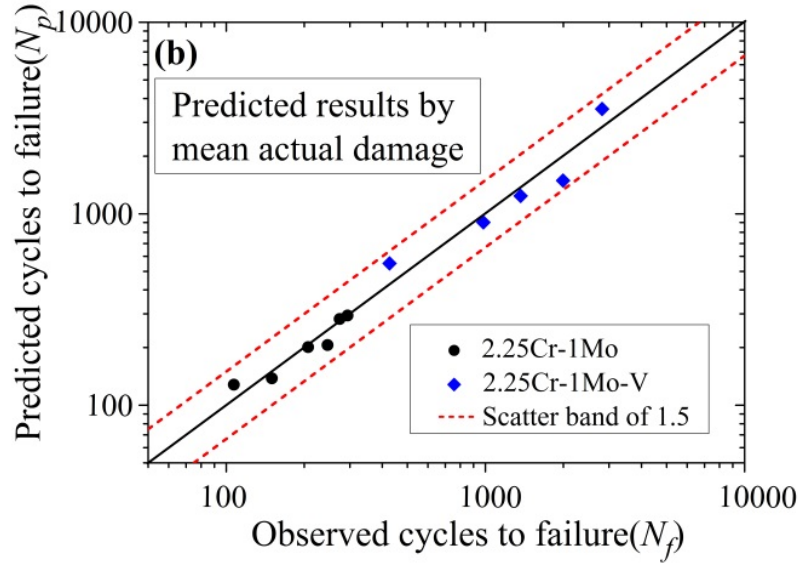

19
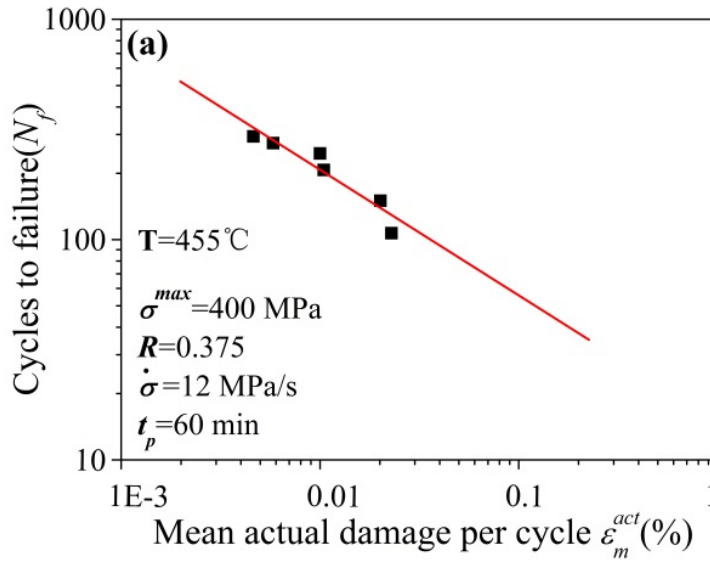
Fig. 14 (a) Liner fitting between mean actual damage during stable stage and cycles to failure and (b) comparison of predicted and observed cycles to failure in cyclic creep under different unloading conditions.

6. Conclusions

Uniaxial stress-controlled static creep and cyclic creep tests of bainite 2.25Cr-1Mo steel have been performed at 455 °C. The tests are conducted under changed unloading conditions, with different unloading rates and durations under valley stress being applied. The principal observations and conclusions of this study are as follows:

1. Compared with static creep, a longer endurance life is observed under cyclic creep. The fracture modes of tested specimens suffer ductile fracture under static creep and cyclic creep which involves a long-term duration of peak stress. The ductility of specimen failed after cyclic creep is slightly lower than that after static creep.
2. The unloading elastic modulus varies with different unloading rate. The anelastic strain during the unloading period shows dependence on both unloading rate and valley stress duration. Based on strain classification, the evolution of the strain (ε^r, ε^c) and the recovery strain (ε^e, ε_{un}^{an}, and ε_v^{an}) with cyclic life under different unloading conditions can be divided into distinct stages, which are found to enter the stable evolution stage after the first cycle.
3. The actual damage created per cycle is systematically considered by the classified strain components during the stable stage. By introducing the difference between maximum strain and recovery strains as a damage parameter, a fatigue life prediction method is proposed. The model provides satisfactory estimated results for cyclic creep loading conditions.

Acknowledgement

Author contributions

Hao Jiang wrote the paper and completed cyclic creep tests. O. O. Ogunmola completed SEM observation. Zizhen Zhao reviewed and revised the paper. Xu Chen guided the research and revised the paper.

References

1. Okrajni J, Cie M, Swad L. High-temperature low-cycle fatigue and creep behaviour of nickel-based super-alloys with heat-resistant coatings. *Fatigue Fract Eng Mater Struct* . 2020; 21(8):947-954.

2. Li C, Chen G, Chen X, Zhang W. Ratcheting strain and simulation of 16MnR steel under uniaxial cyclic loading. *Comput Mater Sci* . 2012;57:43-47.

3. Kubena I, Polak J, Plocinski TP, Hebert C, Skorik V, Kruml T. Microstructural stability of ODS steels in cyclic loading. *Fatigue Fract Eng Mater Struct* . 2015; 38(8): 936-947.

4. Raman SGS, Argence D, Pineau A. High temperature short fatigue crack behaviour in a stainless steel. *Fatigue Fract Eng Mater Struct* . 2010; 20(7):1015-1031.

5. Kordisch T, Nowack H. Life prediction for the titanium alloy imi 834 under high temperature creep–fatigue loadings. *Fatigue Fract Eng Mater Struct* . 1998; 21(1): 47-63.

6. Barua B, Mohanty S, Listwan JT, Majumdar S, Natesan K. Methodology for Stress-Controlled Fatigue Test Under In-Air and Pressurized Water Reactor Coolant Water Condition and to Evaluate the Effect of Pressurized Water Reactor Water and Loading Rate on Ratcheting. *J Press Vess Technol.* 2018;140(3):031403-1-7.

7. Oldroyd PWJ, Radon JC. Reversal of cyclic creep in mild steel and copper. *Fatigue Fract Eng Mater Struct* . 2010;1(3):297-306

8. Raman SGS, Argence D, Pineau A. High temperature short fatigue crack behaviour in a stainless steel. *Fatigue Fract Eng Mater Struct* . 2010;20(7):1015-1031.

9. Luo H, Kang G, Kan Q, Ma C. Experimental study on the whole-life heterogeneous ratchetting and ratchetting-fatigue interaction of SUS301Lstainless steel butt-welded joint. *Fatigue Fract Eng Mater Struct* . 2020;4:36-50

10. Zhao P, Xuan F. Ratchetting behaviorbehaviourbehaviour of advanced 9-12% chromium ferrite steel under creep-fatigue loadings: Fracture modes and dislocation patterns. *Mater Sci Eng: A*2012;539:301-307.

11. Zhao P, Xuan F. Ratchetting behavior of advanced 9-12% chromium ferrite steel under creep-fatigue loadings. *Mech. Mater.*2011;43(6):299-312.

12. Hu D, Ma Q, Shang L, Gao Y, Wang R. Creep-fatigue behaviour of turbine disc of superalloy GH720Li at 650°C and probabilistic creep-fatigue modeling. *Mater Sci Eng: A.* 2016;670:17-25.

13. Matejczyk DE, Zhuang Y, Tien JK. Anelastic relaxation controlled cyclic creep and cyclic stress rupture behaviour of an oxide dispersion strengthened alloy. *Metall Trans A.* 1983;14(1):241-247.

14. Hu X, Zhang Q, Jiang Y, Rao G, Miao G, He W, et al. The effect of cyclic loading on the creep fatigue life and creep strength of a DS superalloy: Damage mechanism and life modeling. *Int J Fatigue* . 2020;134:105452.1-105452.14.

15. Hong KT, Lee JK, Nam SW. Threshold stress for cyclic creep acceleration in copper. *J Mater Sci.* 1988;23(5):1569-1572.

16. Yasnii PV, Halushchak MP, Fedak SI, Pidkol'zinet VY. Cyclic creep of AMG6 alloy. *Mater Sci.* 2000;36(1):48-53.

17. Wang Z, Rahka K, Laird C. Cyclic creep acceleration and retardation in cr-mo-v rotor steel at ambient and elevated temperature respectively.*Fatigue Fract Eng Mater Struct* . 2010;9(3):219-230.

18. Bonisch M, Calin M, Humbeeck JV, Skrotzki W, Eckert J. Factors influencing the elastic moduli, reversible strains and hysteresis loops in martensitic Ti-Nb alloys. *Mater Sci Eng: C.* 2015;48:511-520.

19. Zhang S, Xuan F, Guo S, Zhao P. The role of anelastic recovery in the creep-fatigue interaction of 9-12% Cr steel at high temperature.*Int J Mech Sci.* 2017;122:95-103.

20. Gaudin C, Feaugas X. Cyclic creep process in AISI 316L stainless steel in terms of dislocation patterns and internal stresses. *Acta Mater.* 2004;52(10):3097-3110.

21. Rao A, Bouchard PJ, Northover SM, Fitzpatrick ME. Anelasticity in austenitic stainless steel. *Acta Mater.* 2012;60(19):6851-6861.

22. Nardone VC, Kimmerle WL, Tien JK. Cyclic creep and anelastic relaxation analysis of an ODS superalloy. *Metall Mater Trans A.*1986;17(9):1577-1583.

23. Reynolds GL, Beeré WB, Burton B. The configuration and climb rate of dislocation links and the contribution to ane-lastic creep. *Met Sci.* 1977;11(6):213-218.

24. Gibeling JC, Nix WD. Observations of anelastic backflow following stress reductions during creep of pure metals. *Acta Metall.*1981;29(10):1769-1784.

25. Sawada K, Kimura K, Abe F. Mechanical response of 9% Cr heat-resistant martensitic steels to abrupt stress loading at high temperature. *Mater Sci Eng: A.* 2003;358(1–2):52-58.

26. Gibeling JG, Nix WD. A numerical study of long range internal stresses associated with subgrain boundaries. *Acta Metall.*1980;28(12):1743-1752.

27. Hosseini E, Kalyanasundaram V, Li X, Holdsworth SR. Effect of prior deformation on the subsequent creep and anelastic recovery behaviour of an advanced martensitic steel. *Mater Sci Eng: A.* 2018;717:68-77.

28. Klueh RL. Heat treatment effects on creep and rupture behaviour of annealed 2.25 Cr-1 Mo steel. *Metall Mater Trans.*1978;9A:1591-1598.

29. Jaske CE. Fatigue curve needs for higher strength 2-1/4Cr-1Mo steel for petroleum process vessels. *J Press Vess Technol.*1990;112:323-332,.

30. Challenger KD, Miller AK, Brinkman CR. An Explanation for the Effects of Hold Periods on the Elevated Temperature Fatigue Behaviour of 2 1/4 Cr-1 Mo Steel. *J Eng Mater Technol.* 1981;103(1):7-14.

31. Challenger KD, Miller AK, Langdon RL. Elevated temperature fatigue with hold time in a low alloy steel: A predictive correlation. *J Mater Eng.* 1981;3(1):51-61.

32. Kschinka BA, Stubbins JF. Creep-fatigue-environment interaction in a bainitic 2.25wt.%Cr-1wt.%Mo steel forging. *Mater Sci Eng: A.*1989;110:89-102.

33. Zhang J, Yu D, Zhao Z, Zhang Z, Chen G, Chen X. Low cycle fatigue of 2.25Cr1Mo steel with tensile and compressed hold loading at elevated temperature. *Mater Sci Eng: A.* 2016;667:251-260.

34. Zhao Z, Yu D, Chen G, Chen X. Ratcheting-fatigue behaviour of bainite 2.25Cr1MoV steel with tensile and compressed hold loading at 455. *Fatigue Fract Eng Mater Struct .* 2019;42(9):1937-1949.

35. Kim WG, Park JY, Ekaputra IMW, Kim SJ, Jang J. Cyclic creep behaviour under tension-tension loading cycles with hold time of modified 9Cr-1Mo steel. *Mater High Temp.* 2014;31(3):249-257.

36. Bee JV, Howell PR, Honeycombe RWK. Isothermal transformations in iron-chromium- carbon alloys. *Metall Mater Trans A.*1979;10(9):1207-1212.

37. Kuo KH, Jia CL. Crystallography of $M_{23}C_6$ and M_6C precipitated in a low alloy steel. *Acta Metall.*1985;33(6):991-996.

38. Fischer T, Kuhn B. Influence of steam atmosphere on the crack propagation behaviour of a 9-12% Cr ferritic/martensitic steel at temperatures from 300 degC to 600 degC depending on frequency and hold time. *Int J Fatigue.* 2019;119:62-77.

39. Fischer T, Kuhn B. Impact of frequency, hold time and atmosphere on creep-fatigue of a 9-12% Cr steel from 300 degC-600 degC. *Int J Fatigue.* 2019;124:288-302.

40. Zheng X, Wu K, Wang W, Yu J, Xu J, Ma L. Low cycle fatigue and ratcheting behaviour of 35CrMo structural steel at elevated temperature.*Nucl Eng Des.* 2017;314:285-292.

41. Zheng X, Wang J, Gao J, Ma L, Yu J, Xue J. Rate-dependent low cycle fatigue and ratcheting of 25Cr2MoVA steel under cyclic pulsating tension. *Mater High Tem.* 2017;35(5):1-8.

42. Chen M, Lin Y, Li K, Chen J. The nonlinear unloading behaviour of a typical Ni-based superalloy during hot deformation: a new elasto-viscoplastic constitutive model. *Appl Phys A.*2016;122(9):869.1-869.12.

43. Chen M, Lin Y, Li K, Chen J. The nonlinear unloading behaviour of a typical Ni-based superalloy during hot deformation: a unified elasto-viscoplastic constitutive model. *Appl Phys A* . 2016;122(9):854.1-854.14.

44. Kim H, Kim C, Barlat F, Pavlina E, Lee MG. Nonlinear elastic behaviours of low and high strength steels in unloading and reloading.*Mater Sci Eng: A.* 2013; 562: 161-171.

45. Zheng X, Xuan F, Zhao P. Ratcheting-creep interaction of advanced 9-12% chromium ferrite steel with anelastic effect. *Int J Fatigue.* 2011;33(9):1286-1291.

46. Yang M, Akiyama Y, Sasaki T. Evaluation of change in material properties due to plastic deformation. *J Mater Process Technol.*2004;151(1-3):232-236.

47. Stefani JA, Nardone VC, Tien JK. On the refinement of the anelastic relaxation controlled cyclic creep model. *Scripta Metall.* 1986; 20(5):685-688.

48. Mareau C, Favier V, Weber B, Galtier A, Berveiller M. Micromechanical modeling of the interactions between the microstructure and the dissipative deformation mechanisms in steels under cyclic loading. *Int J Plast.* 2012; 32-33: 106-120.

49. Liu X, Shiwa M, Sawada K, Yamawaki H, Watanabe M, Yin F. Effect of cold working deformation on the internal friction of 2.25Cr-lMo steel.*Mater Sci Eng: A.* 2010; 527(24-25):6741-6744.

50. Morris DG. Anelasticity and creep transients in an austenitic steel.*J Mater Sci.* 1978;13(9):1849-1854.

51. Fan Z, Chen X, Chen L, Jiang J. Fatigue-creep behaviour of 1.25Cr0.5Mo steel at high temperature and its life prediction. *Int J Fatigue.* 2007;29(6):1174-1183.

52. Zhu Y, Kang G, Yu C. A finite cyclic elasto-plastic constitutive model to improve the description of cyclic stress-strain hysteresis loops. *Int J Plast.* 2017;95:191-215.

53. R5 assessment procedure for the high temperature response of structures. British Energy Genation. UK, 2010.